# Simulation Approaches for Burn Severity Estimation Using Remotely Sensed Images

**Emilio Chuvieco[1,3,*], Angela De Santis[1], David Riaño[1,2] and Kerry Halligan[3]**

[1]Department of Geography, University of Alcalá
Calle Colegios 2, Alcalá de Henares, Madrid 28801, Spain

[2]Center for Spatial Technologies and Remote Sensing, University of California, Davis
250-N, The Barn, One Shields Avenue, Davis, CA 95616 (USA).

[3]Department of Geography, University of California, Santa Barbara
3611 Ellison Hall, Santa Barbara, CA 93106 (USA)

[*]Corresponding author: Tel.: +34-918854438; e-mail: emilio.chuvieco@uah.es

## ABSTRACT

Traditional field-based methods for estimating burn severity are time-consuming, labour intensive and normally limited in spatial extent. Remotely sensed data provide a means to estimate severity levels across large areas, but it is critical to understand the causes of variability in spectral response with variations in burn severity. Since experimental measurements over a range of burn severities are difficult to obtain, the simulation tools provided by radiative transfer models (RTM) offer a promising alternative to better understand factors affecting burn severity reflectances. Two-layer RTM, such as the combined leaf (Prospect) and canopy (Kuusk) model can be used to simulate a wide range of burn severity conditions. Specifically, the effects of changes in soil background, leaf color and leaf area index as a result of different burn severities can be simulated with two-layer RTM models in the forward mode. This approach can provide a deeper understanding of the effects of each factor in satellite-sensed reflectance, as well as their relative importance. Additionally, RTMs can also be used in an inverse mode, and therefore burn severities can be retrieved from remotely sensed data by comparing measured and simulated reflectance.

Examples of these two-way modes of RTMs are presented in this paper. Burn severity was measured using the Composite Burn Index (CBI). The Kuusk model was used to simulate scenarios of different combinations of changes in the substrate, upper vegetation, and lower vegetation strata. This paper shows some results of inverting the simulated reflectances to estimate CBI from calibrated reflectance derived from different satellite sensors. The case study is based on a large forest fire that affected central Spain in July, 2005. Landsat-TM, SPOT-HRV, IRS-AWIFS, Envisat-MERIS and Terra-MODIS data were used for this retrieval. Determination coefficients ($r^2$) values range between 0.436 (MODIS) to 0.629 (Landsat-TM), with lower precision for the intermediate range of CBI values.

*Keywords:* burn severity, fire effects, forest fires, radiative transfer models, reflectance

*Citation:* Chuvieco, E., A. De Santis, D. Riaño and K. Halligan. 2007. Simulation approaches for burn severity estimation using remotely sensed images. Fire Ecology 3(1): 129-150.

## INTRODUCTION

Discrimination of different degrees in post-fire effect assessment is critical to improve management of fire-affected areas, either to help natural regrowth, reduce soil erosion and degradation, or improve landscape diversity (Key 2005, Lachowski *et al.* 1997, Lentile *et al.* 2006, Turner *et al.* 1994). Additionally, the degree of biomass consumed by the fire is one of the key factors to estimate gas emissions derived from wildland fires (Chuvieco *et al.* 2004, Epting *et al.* 2005, Michalek *et al.* 2000).

In recent years, several papers have tried to clarify the terminology of post-fire effects assessment (Jain and Graham 2004, Lentile *et al.* 2006). Following these papers, the term burn severity will be used throughout this paper to refer to the analysis of post-fire characteristics of vegetation and substrate after the fire is fully extinguished. When referring to other papers, we will try to convert their terminology to this one, based on this "what is left after the fire" concept.

Several authors have proposed field methods to discriminate burn severity based on quantitative or qualitative criteria (Key and Benson 2005, Lentile *et al.* 2006, Miller and Yool 2002, Moreno and Oechel 1989, Pérez and Moreno 1998). These methods are laborious and costly and present severe obstacles to be spatially representative. Remotely sensed images have been used as an alternative because they provide a spatial comprehensive view, are cost-efficient, and provide up to date information on landscape conditions. In the last years, a large number of papers have explored the use of remote sensing in burn severity assessment (Brewer *et al.* 2005, Cocke *et al.* 2005, Díaz-Delgado *et al.* 2003, Díaz-Delgado *et al.* 2001, Epting *et al.* 2005, Kachmar and Sanchez-Azofeifa 2006, Key 2005, Michalek *et al.* 2000, Miller and Yool 2002, Parra and Chuvieco 2005, Rogan and Franklin 2001, Rogan and Yool 2001, Roy and Landmann 2005, Roy *et al.* 2006, Ruiz-Gallardo 2004, Sa *et al.* 2005, van Wagtendonk *et al.* 2004, White *et al.* 1996). These papers covered a range of different techniques: spectral indices, principal components, classification, multitemporal change detection, etc. Although most rely on Landsat-TM/ETM+ data, there are also some examples of hypespectral data (Parra and Chuvieco 2005, van Wagtendonk *et al.* 2004).

One of the main difficulties of using these studies for global assessment of burn severity from remotely sensed data is the empirical approach that has guided most studies published so far. Empirical models are simple to calibrate and provide a quantitative estimation of burn severity, but they provide little confidence on whether they are applicable or not to other ecosystems or fuel characteristics.

For this reason, the use of alternative tools for interpreting remotely sensed data is desirable. In recent years, physical models have been proposed as a viable alternative to derive quantitative information from reflectance calibrated images. Successful application of these models has been reported in the estimation of chlorophyll (Zarco-Tejada *et al.* 2001), moisture content (Danson and Bowyer 2004), and dry matter (Riaño *et al.* 2005). Simulation models attempt to account for the effects of different factors that modify plant reflectance and transmittance: chemical composition, geometrical configuration, illumination and observation angles, etc. The large number of proposed models can be classified into general groups depending on their main assumptions: turbid medium models, geometrical models, stocastic models and ray-tracing models (Liang 2004). Most common models are based on the radiative transfer equation and therefore are named radiative transfer models (RTM) since they account for the multiple scattering of radiation as it interacts with the vegetation canopy and soil background. Such interaction can be modeled assuming that the vegetation represents one or more homogenous layers. Other possibilities include the consideration of discontinuous canopies, such as row structure in crops or grid structure in tree plantations,

and higher levels of complexity such as the consideration of three-dimensional vegetation structure models (Pinty *et al.* 2004). Although more complex models are closer to reality than those based on homogeneous canopies, they require a large number of input variables, making them harder to parameterize with real data.

Models can be used in forward and backward approaches (Liang 2004). The former implies changing the input parameters to simulate the effects of those changes in the final reflectance. The latter inverts the given model, such that the input parameters that generated an observed reflectance spectrum may be estimated.

Burn severity studies have made very little use of simulation models so far. Roy *et al.* (2005, 2002) used a RTM to simulate reflectance from burned and unburned areas for different view and illumination angles of MODIS data. Their goal was to obtain an automatic algorithm for mapping burned areas from multitemporal acquisitions of MODIS data. Pereira *et al.* (2004) used a mixed geometrical-turbid medium model to simulate whether understory fires could be detectable in the Miombo woodlands at different tree densities. A forward RTM simulation for burn severity was recently proposed by Chuvieco *et al.* (2006) to identify the most sensitive wavelength regions for burn severity retrieval from remote sensing imagery. DeSantis and Chuvieco (2006) compared the results of inverting this simulation model with those obtained from an empirical model in the retrieval of burn severity values from Landsat-TM images. Results from this inversion showed a good agreement in the upper and lower part of the severity range, while more error occurred in the central values.

The objectives of this paper are twofold. First we tried to extend the RTM simulations previously published (Chuvieco *et al.* 2006) by including a wider range of scenarios and input conditions, with the goal of improving the middle range of the severity scale. The second objective was to extend the estimations provided by model inversion (De Santis and Chuvieco, 2006) to other sensors, including both higher spatial resolution data: Landsat-TM, SPOT-HRV and IRS-AWIFS; and lower: Envisat-MERIS and Terra-MODIS.

## METHODS

### *Reference Burn Severity Measure*

Among the different procedures to measure burn severity, we selected the Composite Burn Index (CBI) as the target estimation variable. The CBI was originally proposed by Key and Benson in 1999 (Key and Benson 2005) and was intended to provide a quantitative estimation of burn severity that could be derived from satellite data. The index was developed within the FIREMON project and has been widely used by researchers using satellite data for mapping burn severity (Cocke *et al.* 2005, De Santis and Chuvieco 2006, Epting *et al.* 2005, Key 2005, Lentile *et al.* 2006, Parra and Chuvieco 2005)

The CBI provides a semi-quantitative index of severity instead of using qualitative ranges (high, medium, low) commonly adopted by other authors. This numerical rating facilitates the statistical validation of the estimates derived from quantitative remotely sensed data. The CBI is based on evaluating different variables associated with fire effects in different strata of a field plot. The observations can be performed quickly and easily in the field, therefore maximizing the number of plots that can be sampled with a fixed field effort. Five strata are evaluated in the CBI: A: substrate (material lying on the floor); B: herbs, short shrubs and small trees (<1 m tall); C: tall shrub and sapling trees (<5 m tall); D: intermediate trees (5 m to 20 m tall); and E: large trees (>20 m tall). The first three are used to compute the CBI value of the understory of the plot (A+B+C), while the last two form the overstory (D+E). The final CBI for each plot is the average of all strata, if they are present in that plot (A+B+C+D+E), or otherwise the average of the strata present.

The CBI score of each stratum is estimated after visual inspection of the plot, considering several variables, including: % litter consumed, % foliage consumed, % living or resprouting species, % green or brown leaves, height of charring, % canopy mortality (Key and Benson 2005). A burn severity scale, adapted to each sampled variable, is used to quantify the impact from 0 (no effect) to 3 (highest effect).

### *RTM Model Selection*

The selection of the RTM for our study was based on the input requirements of the burn severity estimation. The model should be sensitive to burn severity variations in different vegetation layers, since CBI scores take into account five strata. From the available RTM in the literature, the Kuusk Markov Chain Canopy Reflectance Model (MCRM) was selected (Kuusk 2001) bcause it allows consideration of two vegetation canopies. It could therefore be used to model any scenario with variations of soil substrate and two vegetation layers. This would be the case when a tree canopy (with different levels of fire effects) has shrubs below (also with various levels of fire efects), as well as a mixture of soil and charcoal in the background.

The Kuusk model considers that the vegetation is homogeneously distributed for each layer and uses leaf optical properties derived from the PROSPECT model (Jacquemoud 1990). The canopy directional reflectance is generated based on the single-scattering and diffuse fluxes from each layer, using direct and diffuse solar irradiance.

One alternative to the Kuusk model would have been to use an RTM that considers the three-dimensional structure of the vegetation such as Forest Light Interaction model (FLIGHT) (North 1996), Discrete Anisotropic Radiative Transfer model (DART) (Gastellu-Etchegorry *et al.* 1996, Gastellu-Etchegorry *et al.* 2004) or Geometric Optical Radiative Transfer model (GORT) (Li *et al.* 1995, Ni *et al.* 1999). Although these models can provide a more realistic characterization of heterogeneous vegetation canopies with individuals of various sizes and fire severity levels, they are also much more complex to parameterize. The more simplistic Kuusk model, on the other hand, is more easily parameterized due to its assumptions of homogenous canopies, while still providing sufficient complexity through its inclusion of two vegetation layers with independent input conditions. This model, therefore, it is well suited to the vertical stratification of observed burn severity levels.

### *Input Conditions to Simulate CBI Values*

To simulate CBI values with the Kuusk model, the four vegetation strata of the CBI approach were reduced to two (Figure 1): the B and C strata of the CBI were identified with low vegetation (lower canopy of the Kuusk model) and D and E strata were assumed to be the upper canopy in the Kuusk model. The CBI A (substrate) was considered as the soil background of the Kuusk model. Each simulation had a corresponding CBI value, following the original FIREMON criterion where the CBI of the plot is a simple average of the CBI for the five strata (three in our case).

CBI is designed to measure burn severity from a set of variables that are critical in assessing fire effects. However, not all of them can be simulated with reflectance models, and therefore a further simplification of the CBI components was required for this study. The variables that were taken into account for the simulations were: change in soil substrate, percentage of foliage altered, and percentage change in vegetative cover. These variables were included in the Kuusk model as described by Chuvieco *et al.* (2006). The input spectra for the simulations were either measured using a GER-2600 spectroradiometer (Geophysical & Environmental Research Corporation, Millbrook, NY) or taken from LOPEX database (Hosgood *et al.* 1994). The former

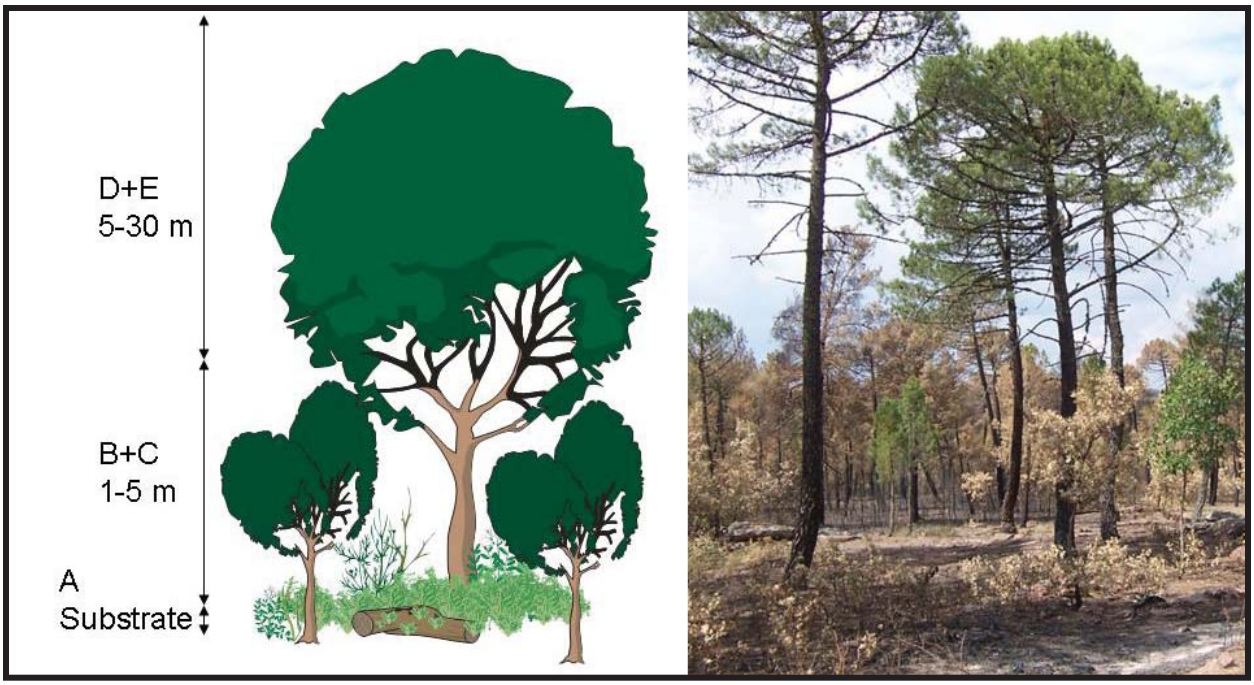


**Figure 1.** Vegetation strata of the CBI (left) and photograph of an area recently burned (right) in the fire used in this paper as study case.

was the case for soil, ash, and charcoal spectra, while the latter was the case for the green and brown leaf spectra (Figure 2). Variations in leaf color (PFA) and canopy cover (PCC) were simulated from the Kuusk model by assuming different proportions of green versus brown leaves and changing the Leaf Area Index (LAI), respectively (Chuvieco *et al.* 2006). LAI thresholds for full cover of vegetation were fixed at 2 for the lower stratum and 3 for the upper one. These values were based on LAI values for typical Mediterranean shrubs derived from the literature (Scurlock *et al.* 2001) and from our own field data. CBI values for each stratum were computed using the thresholds defined in the FIREMON protocol, while intermediate values were obtained using linear interpolation.

### *Simulation Scenarios*

Several simulation scenarios were considered to account for the diversity of post-fire severity conditions and the complexity of potential pre- and post-fire changes. Four scenarios were considered:

1. Single post-fire, assuming that fire causes simultaneous leaf consumption and leaf browning.
2. Extended post-fire, supposing that fire may either consume the leaves or brown them or both.
3. Multitemporal, by modeling changes in leaf color and cover from fixed pre-fire conditions.
4. Supervised approach, by selecting the most commonly found combinations of input parameters from field experience.

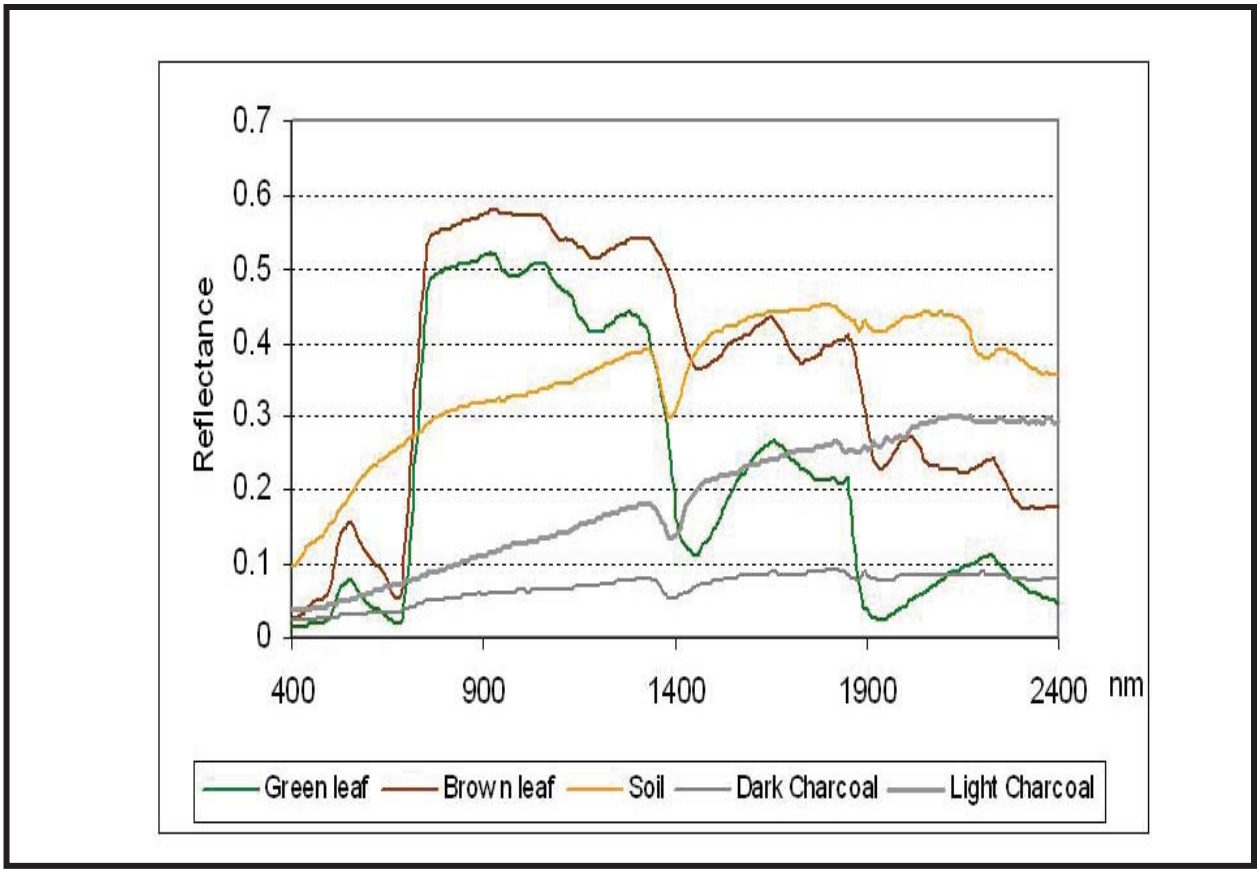


**Figure 2.** Input spectra used in the simulations.

The first scenario was the simplest, assuming that changes in leaf color and leaf cover occurred in parallel. In other words, the larger the fire effect, the browner the leaves and the lower the leaf area index were (Figure 3). To simulate this scenario, ten different cases for each stratum were considered, as indicated in Table 1. From the 1,000 output cases, several filters were applied to avoid unrealistic combinations of CBI values for the different strata (high crown CBI and very low CBI underneath, for instance) following our field observations (Chuvieco *et al.* 2006, De Santis and Chuvieco 2006)

The second scenario assumed an independent variation of PFA and PCC, which implied that leaves could become brown and still remain on the tree, or that the LAI could be reduced while the remaining leaves maintained their green color (Figure 3). Unlike in the first scenario, the soil substrate in the second scenario included not only charcoal and soil, but ash as well. Ash, which is the result of a full combustion process, is very important in the initial post-fire spectral response, as several authors have pointed out (Pereira *et al.* 1999, Trigg and Flasse 2000). However, the ash signal is very ephemeral, because ash is commonly blown away by the wind within a few days following a fire. For the second scenario, 19 combinations of soil, ash and carbon were selected (Table 2). For the PFA and PCC, seven combinations of each were chosen for each stratum. Therefore, a total of 49 cases were considered in the two vegetation strata. The result of varying the substrate conditions plus the two vegetation strata created a total of 45,619 output cases. The same filters as in the first scenario were applied, including an extra one to remove unrealistic combinations of PFA and PCC. Cases with a high consumption of leaves (high PCC) are very unlikely to occur

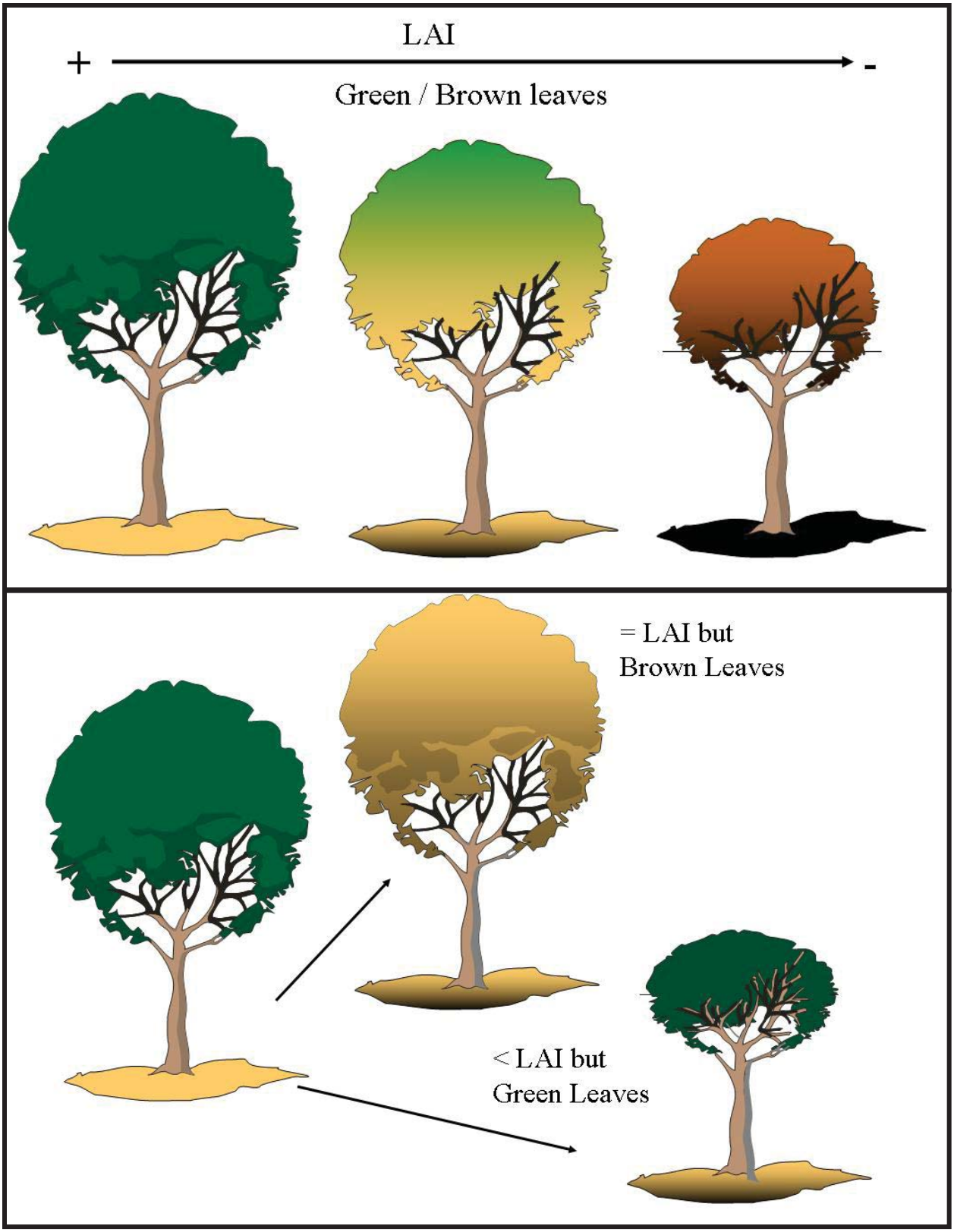


**Figure 3.** Simulation strategies: top, PFA and PCC change simulteneously; bottom, PFA and PCC change independently.

**Table 1.** Input parameters for the first simulation scenario (Chuvieco *et al.* 2006).

| A | | B+C | | | D+E | | |
|---|---|---|---|---|---|---|---|
| **CBI** | **% burned soil** | **CBI** | **% dry leaves** | **LAI value** | **CBI** | **% dry leaves** | **LAI value** |
| 0.00 | 0.0 | 0.00 | 0.0 | 2.00 | 0.00 | 0.0 | 3.00 |
| 0.33 | 3.3 | 0.50 | 5.0 | 1.85 | 0.50 | 5.0 | 2.78 |
| 0.67 | 6.7 | 1.00 | 10.0 | 1.70 | 1.00 | 10.0 | 2.55 |
| 1.00 | 10.0 | 1.33 | 24.9 | 1.34 | 1.33 | 24.9 | 2.01 |
| 1.33 | 19.9 | 1.67 | 40.2 | 0.96 | 1.67 | 40.2 | 1.44 |
| 1.67 | 30.1 | 2.00 | 55.0 | 0.60 | 2.00 | 55.0 | 0.9 |
| 2.00 | 40.0 | 2.25 | 72.5 | 0.40 | 2.25 | 72.5 | 0.60 |
| 2.33 | 53.2 | 2.50 | 90.0 | 0.20 | 2.50 | 90.0 | 0.30 |
| 2.67 | 66.8 | 2.75 | 95.0 | 0.11 | 2.75 | 95.0 | 0.16 |
| 3.00 | 80.0 | 3.00 | 100.0 | 0.01 | 3.00 | 100.0 | 0.01 |

**Table 2.** Variations of background for the second simulation scenario.

| Case | % charoal | % ash | % soil |
|---|---|---|---|
| 1 | 0.00 | 0.00 | 100.00 |
| 2 | 5.00 | 0.00 | 95.00 |
| 3 | 3.75 | 1.25 | 95.00 |
| 4 | 2.50 | 2.50 | 95.00 |
| 5 | 10.00 | 0.00 | 90.00 |
| 6 | 7.50 | 2.50 | 90.00 |
| 7 | 5.00 | 5.00 | 90.00 |
| 8 | 25.00 | 0.00 | 75.00 |
| 9 | 18.75 | 6.25 | 75.00 |
| 10 | 12.50 | 12.50 | 75.00 |
| 11 | 40.00 | 0.00 | 60.00 |
| 12 | 30.00 | 10.00 | 60.00 |
| 13 | 20.00 | 20.00 | 60.00 |
| 14 | 70.00 | 0.00 | 30.00 |
| 15 | 52.50 | 17.50 | 30.00 |
| 16 | 35.00 | 35.00 | 30.00 |
| 17 | 100.00 | 0.00 | 0.00 |
| 18 | 75.00 | 25.00 | 0.00 |
| 19 | 50.00 | 50.00 | 0.00 |

without any change in leaf color (low PFA). Linear regressions between $PCC_e$ and PFA in each stratum were derived from our field data. These linear models were then applied to the simulation cases, and cases with high residuals eliminated. These linear models were as follows:

$PCC_e = PFA*0.9188 + 0.2858$ for the lower vegetation, and

$PCC_e = PFA*0.8912 – 0.0008$ for the upper vegetation layer

Cases with higher or lower PCC than ± $PCC_e$ were eliminated. A total of 4,100 cases remained after applying all these filters.

In both of the two first scenarios, it was assumed that before the fire the understory and the overstory had the maximum LAI values (2 and 3, respectively). In other words, we modeled the fire effects in a high-density forest area. Therefore, lower LAI values were assumed to be caused by higher burn severity (leaf losses as a result of the fire) and not by lower leaf density before the fire. This may not be realistic in those forested areas where recent fires or forestry clearing have occurred.

A third simulation scenario considered the changes in spectral reflectance from before to after the fire. While the same number of simulation cases was used for the post-fire condition as in the second scenario, only four pre-fire cases with medium to high LAI values and full green leaves were considered in both the lower and upper vegetation strata. This was done to avoid a large number of combinations derived from very different pre-fire conditions. Changes in PFA and PCC from those four pre-fire conditions were modeled by substracting simulated post-fire reflectances of the second scenario from the four pre-fire simulated reflectance spectra (Tables 3a, 3b and 3c). Likewise, the image that was inverted was a pre-fire minus post-fire image. In this scenario, any changes in LAI are more soundly related to changes in canopy cover as a result of fire consumption than when using a single post-fire scenario.

All simulations consider a wide range of combinations of the input parameters, which could cause confusion in the model inversion, because similar reflectance properties could be derived from different combinations of input parameters. As a result, similar reflectance patterns would correspond to different CBI values. This situation has been observed in other applications of RTM inversion (Combal *et al.* 2002). For this reason, we considered a fourth simulation scenario that was named post-fire "supervised approach," in which we selected only those input conditions that are the most common in Mediterranean fires, according to our field experience. In other words, instead of using the full range of variation for the input variables, only a limited number of cases were selected. This small set of spectra was extracted from the modeled spectra obtained in the second simulation scenario. It should be stressed that these spectra are derived from the simulations and not from the image, so they are independent of image conditions. Table 4 includes the simulation cases that were selected for our supervised model.

### *Forward and Backward Simulation*

Forward simulation was based on the input parameters described above. All simulations were performed for the spectral range of 400 nm to 2,400 nm, at 10 nm intervals giving a total of 201 spectral bands per modeled spectrum. To reduce model complexity, some variables were kept fixed through all simulations: leaf angle distribution = plagiophile, leaf shape = ellipse form (eccentricity = 0.95), sun zenith angle = 30º, nadir angle = 0, azimuth angle = 0. Forward simulations are useful to analyze the effect of

**Table 3a.** Pre-fire and post-fire conditions for 18 combinations of charcoal, ash, and soil substrates used to simulate multitemporal changes of fire severity. Simulations were conducted by subtracting each post-fire condition from the corresponding pre-fire condition.

| Charcoal | Ash | Soil |
|---|---|---|
| **Pre-fire conditions (%)** | | |
| 0 | 0 | 100 |
| **Post-fire conditions (%)** | | |
| 5.00 | 0.00 | 95.00 |
| 3.75 | 1.25 | 95.00 |
| 2.50 | 2.50 | 95.00 |
| 10.00 | 0.00 | 90.00 |
| 7.50 | 2.50 | 90.00 |
| 5.00 | 5.00 | 90.00 |
| 25.00 | 0.00 | 75.00 |
| 18.75 | 6.25 | 75.00 |
| 12.50 | 12.50 | 75.00 |
| 40.00 | 0.00 | 60.00 |
| 30.00 | 10.00 | 60.00 |
| 20.00 | 20.00 | 60.00 |
| 70.00 | 0.00 | 30.00 |
| 52.50 | 17.50 | 30.00 |
| 35.00 | 35.00 | 30.00 |
| 100.00 | 0.00 | 0.00 |
| 75.00 | 25.00 | 0.00 |
| 50.00 | 50.00 | 0.00 |

**Table 3b.** Pre-fire and post-fire conditions for six combinations of LAI values (PCC) for lower and upper vegetation layers. Pre-fire conditions ranged from medium to low for each layer. Simulations were conducted by subtracting each post-fire condition from the corresponding pre-fire condition.

| Lower vegetation | | | | Upper vegetation | | | |
|---|---|---|---|---|---|---|---|
| Pre-fire conditions (LAI) | | | | Pre-fire conditions (LAI) | | | |
| 2.00 | 1.85 | 1.70 | 1.15 | 3.00 | 2.78 | 2.55 | 1.73 |
| Post-fire conditions | | | | Post-fire conditions (LAI) | | | |
| 1.85 | 1.71 | 1.57 | 1.06 | 2.775 | 2.57 | 2.36 | 1.60 |
| 1.70 | 1.57 | 1.45 | 0.98 | 2.55 | 2.36 | 2.17 | 1.47 |
| 1.15 | 1.06 | 0.98 | 0.66 | 1.725 | 1.60 | 1.47 | 0.99 |
| 0.60 | 0.56 | 0.51 | 0.35 | 0.9 | 0.83 | 0.77 | 0.52 |
| 0.20 | 0.19 | 0.17 | 0.12 | 0.3 | 0.28 | 0.26 | 0.17 |
| 0.01 | 0.01 | 0.01 | 0.01 | 0.01 | 0.01 | 0.01 | 0.01 |

**Table 3c**. Pre-fire and post-fire conditions for six combinations of for leaf color (PFA) for % dry/green leaves, optical thickness, chlorophyll content, brown pigment content, water content, and dry matter content. Simulations were conducted by subtracting each post-fire condition from the corresponding pre-fire condition.

| Dry/green leaves (%) | Optical thickness (unitless) | Chlorophyll content( %) | Brown pigment (%) | Water content( %) | Dry matter (%) |
|---|---|---|---|---|---|
| Pre-fire conditions | | | | | |
| 0.0 | 1.4 | 42 | 30 | 0.0075 | 0.006 |
| Post-fire conditions | | | | | |
| 12.5 | 1.6 | 39 | 34 | 0.0056 | 0.006 |
| 25.0 | 1.8 | 39 | 42 | 0.0050 | 0.006 |
| 43.2 | 1.9 | 34 | 60 | 0.0031 | 0.006 |
| 80.0 | 2.5 | 28 | 91 | 0.0013 | 0.006 |
| 95.0 | 2.9 | 28 | 102 | 0.0006 | 0.006 |
| 100.0 | 3.0 | 28 | 106 | 0.0006 | 0.006 |

input parameters in the simulated reflectance to better understand their importance in the final output, as well as to identify which bands are more sensitive to each input parameter. In our case, we were interested in determining which bands or band combinations were more sensitive to variations in soil substrate, leaf color or leaf cover, as they are combined in the CBI computation.

The simulations generated in the different scenarios can then be related to reflectance values as extracted from satellite data. The most similar spectra between each observed spectrum and the whole range of simulated spectra should provide an estimation of the input parameters that generated that particular spectrum. This is the basis for the inversion of RTM, which is based on minimizing the merit function:

$$\chi^2 = \sum_{i=1}^{n} \left[\rho_i - \mathrm{M}(\Theta - X)\right]^2 \quad (1)$$

where $\chi$ is the difference between the observed reflectance ($\rho$) and the modeled reflectance ($M(\Theta, X)$, for a certain set of input parameters

**Table 4:** Input conditions for the supervised simulation scenario. The CBI value of each stratum may be different regarding leaf conditions (PFA) and canopy cover (PCC) as in the second simulation.

| Average CBI | Lower vegetation | | Upper vegetation | | Substrate | |
|---|---|---|---|---|---|---|
| | % Dry leaves | LAI | % Dry leaves | LAI | CBI A | Type |
| 0.00 | 0 | 0 | 0 | 0 | 0 | Soil |
| 0.00 | 0 | 0 | 0 | 0 | 0 | Soil |
| 0.00 | 25 | 0 | 25 | 0 | 0 | Soil |
| 0.40 | 25 | 1.2 | 0 | 0 | 0 | Charcoal 10% |
| 0.50 | 25 | 1.2 | 25 | 0 | 0 | Charcoal 10% |
| 0.70 | 43 | 0.6 | 25 | 2.78 | 1 | Soil |
| 1.00 | 25 | 0.01 | 25 | 1.8 | 1.5 | Charcoal 100% |
| 1.50 | 43 | 1.2 | 43 | 1.8 | 1 | Charcoal 10% |
| 1.50 | 100 | 1.7 | 100 | 2.55 | 1.5 | Charcoal 100% |
| 1.60 | 95 | 0.01 | 25 | 0.5 | 0 | Charcoal 12.5%+Ash 12.5% |
| 1.70 | 80 | 0.2 | 25 | 2.55 | 3 | Charcoal 25% |
| 1.90 | 80 | 0.6 | 80 | 0.9 | 3 | Charcoal 100% |
| 1.90 | 2.5 | 0.6 | 25 | 1.8 | 1.5 | Charcoal 25% |
| 2.00 | 100 | 0 | 0 | 0.9 | 3 | Charcoal 100% |
| 2.00 | 100 | 1.2 | 100 | 2.55 | 1.5 | Charcoal 25% |
| 2.00 | 95 | 0.6 | 43 | 1.8 | 3 | Charcoal 100% |
| 2.10 | 80 | 0.2 | 95 | 1.8 | 3 | Charcoal 100% |
| 2.30 | 95 | 0.6 | 80 | 0.9 | 3 | Charcoal 100% |
| 2.30 | 100 | 0 | 80 | 0.01 | 3 | Charcoal 100% |
| 2.50 | 95 | 0.01 | 95 | 0.3 | 1.5 | Charcoal 25% |
| 2.70 | 100 | 0.2 | 100 | 0.3 | 3 | Charcoal 100% |
| 2.80 | 100 | 0.01 | 100 | 0.01 | 3 | Charcoal 100% |
| 3.00 | 100 | 0.01 | 100 | 0.01 | 3 | Charcoal 100% |
| 3.00 | 100 | 0.01 | 100 | 0.01 | 3 | Charcoal 100% |
| 3.00 | 0 | 0 | 0 | 0 | 3 | Charcoal 75/Ash 25% |

(Θ, X), with X being the value to be estimated, and n the spectral wavelengths of the input image.

There are several alternatives for model inversion in the literature: iterative processes, neural networks, statistical fitting and previous generation of a look up table (LUT) (Liang 2004). The last one was used in this paper because it is quicker and provides a control scenario for searching for the input parameters. The LUT includes the output from running the RTM for the different simulation scenarios (M(Θ, X) as stated in equation 1), so the inversion process does not need to run the model again, but rather it focuses on finding which observed reflectance spectrum is the most similar to the modeled one.

For the merit function of "similarity," several strategies are used, the most common of which was the minimum quadratic distance (as formulated in equation 1). In this paper, several methods were explored based on hyperspectral methods of classification. The most robust for our purposes was the spectral angle mapper (Kruse *et al.* 1993), which calculates the angle between two spectral vectors with the same

origin and selects, for each pixel in the image, the reference spectrum with the lowest spectral angle. In this case, the reference spectra were produced by the simulations and stored in the LUT along with their CBI value. Once the reference spectrum with the minimum spectral angle was selected, the image pixel was labeled with the CBI value of the reference spectrum.

### *Study Site*

The efficiency of model inversion from the different simulation scenarios was tested using a large forest fire that recently occurred in central Spain (Figure 4). The fire occurred in the middle of July 2005 and was caused by human carelessness under very dry weather conditions: maximum temperature 35 ºC; relative humidity 22%; 30 days since the last rainfall event; wind speed 10-23 Km/h. The fire lasted four days and burned approximately 13,000 ha in an area dominated by pine trees (*Pinus pinaster* L.) mixed with semi-deciduous oaks (*Quercus faginea* Lam. and *Quercus pyrenaica* Willd.) and a marginal sector covered mostly by Mediterranean shrubs (*Cistus ladanifer* L., *Cistus albidus* L., *Rosmarinus officinalis* L., *Juniperus oxycedrus* L., *Rosa canina* L., *Cytisus scoparius* L., and *Lavandula pedunculata* L.). Eleven firefighters died while supressing the fire, which caused a great impact in the national media. The topography of the area is rugged and the altitudes range from 1,100 m to 1,400 m. Rainfall in the region averages 600 mm to 800 mm per year. Maximum and minimum precipitation are recorded in November to December, and in July to August, respectively. The average annual temperature is 12 ºC.

A field campaign to obtain CBI values for the burn area was undertaken between August and September, a few weeks after the fire. Therefore, the measured CBI values reflect the short-term burn severity, using Key's terminology (Key 2005). A total of 110 plots were sampled in the

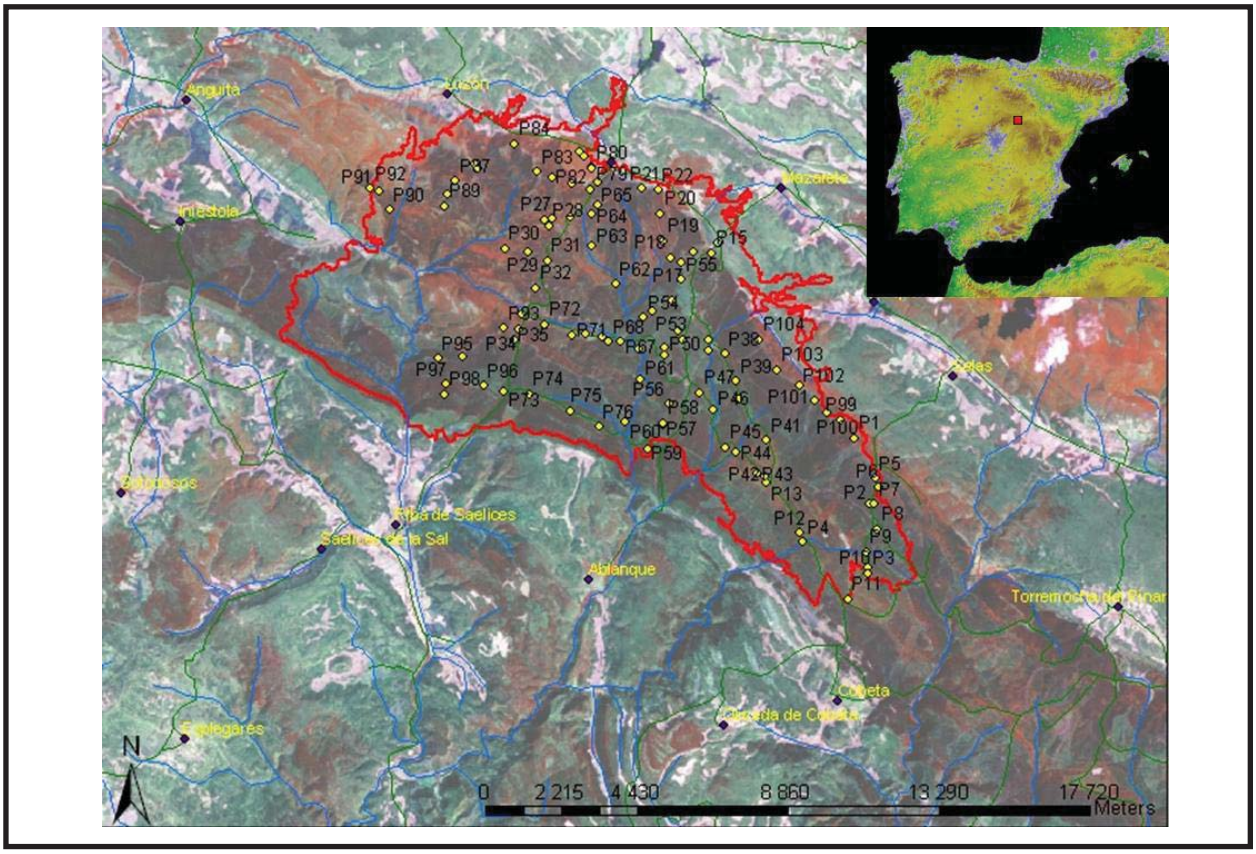


**Figure 4.** Location of the study case.

field using the CBI protocol. Plot coordinates were registered with a Garmin GPS system (GARMIN GPS 12, http://www.garmin.com), with an average precision of ± 10 m. Most of the burn area presented high CBI values. Only 18 out of 110 plots had CBI values lower than 2, and 31 had CBI higher than 2.9. In spite of being a large fire, the severity values did not cover the whole spectrum of possible CBI values, and intermediate levels (CBI between 1 and 2) were uncommon. This imposed a challenge for verifying the performance of the inversion results, as will be discussed later.

### *Image Processing*

Sensors with different spectral and spatial resolution were used for testing the robustness of the model inversion results. Table 5 shows the spatial and spectral characteristics of the images used. In spite of the large differences in spectral and spatial resolution, all images showed a clear and similar pattern in their portayal of the burn area (Figure 5). They were acquired between 15 to 30 days post-fire, except for SPOT-HRV, that was collected 60 days post-fire.

The images were geometrically corrected using reference data extracted from a previously ortho-rectified Landsat image. The SPOT-HRV, Landsat-TM and AWIFS images were converted to radiance using calibration coefficients included in the image header. Atmospheric correction was based on the dark-object method proposed by Chavez (1996). They were also corrected for topographic shade using a variation of the Teillet's C correction method (Riaño *et al.* 2003). MERIS and MODIS images were obtained from the FR2P-level 02 product and the standard MOD09 reflectance product respectively, which include radiometric calibration and atmospheric correction.

**Table 5.** Spatial resolution (m) and center wavelength (μm) of the sensors used for this study.

| Band | Sensor | | | | |
|---|---|---|---|---|---|
| | SPOT-HRV | LANDSAT-TM[2] | IRS-AWIFS | ENVISAT-MERIS | TERRA-MODIS |
| | Spatial resolution (m) | | | | |
| | 10 / 20 | 30 | 60 | 300 | 500 |
| | μm | | | | |
| 1 | 0.545 | 0.487 | 0.555 | 0.413 | 0.469 |
| 2 | 0.645 | 0.571 | 0.650 | 0.442 | 0.555 |
| 3 | 0.835 | 0.661 | 0.815 | 0.490 | 0.645 |
| 4 | 1.675[1] | 0.837 | 1.625 | 0.510 | 0.857 |
| 5 | | 1.677 | | 0.560 | 1.240 |
| 6 | | Thermal[2] | | 0.620 | 1.640 |
| 7 | | 2.215 | | 0.665 | 2.130 |
| 8 | | | | 0.681 | |
| 9 | | | | 0.709 | |
| 10 | | | | 0.754 | |
| 11 | | | | 0.778 | |
| 12 | | | | 0.865 | |
| 13 | | | | 0.885 | |

[1]HRV 1.675 μm band has 20 m resolution. [2]Landsat-TM thermal band was not considered.

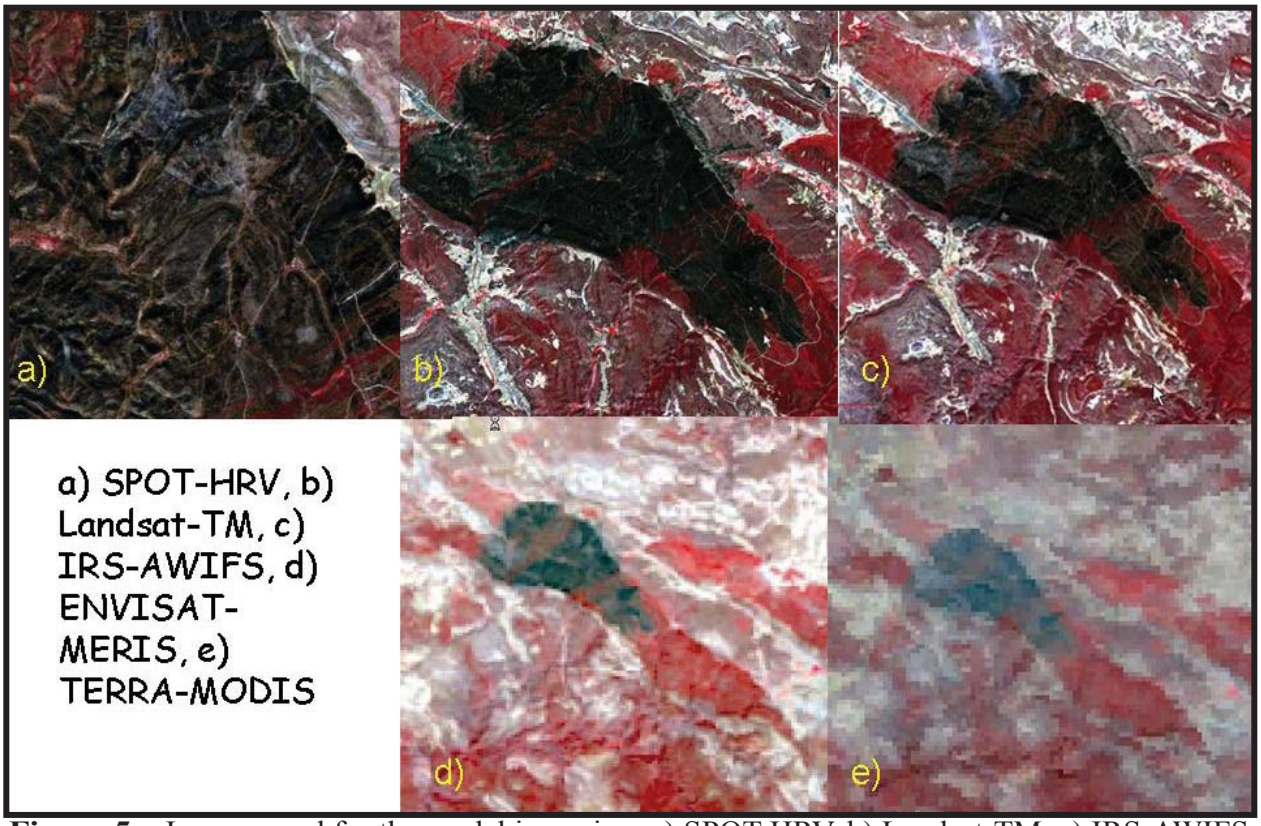


**Figure 5.** Images used for the model inversion: a) SPOT-HRV, b) Landsat-TM, c) IRS-AWIFS, d) ENVISAT-MERIS, e) TERRA-MODIS.

## RESULTS

### *Comparison of Simulated and Actual Reflectances*

To simplify the comments, comparison of simulated and observed reflectances will be based on Landsat-TM images because it provides the best compromise between spatial and spectral resolution from our image dataset.

Figure 6 shows the spectral reflectance of simulated and actual spectra for a set of sample ranges of CBI values from the supervised post-fire simulation. The image spectra were extracted from the post-fire Landsat-TM image. It is noticeable that the observed reflectance for the lower values of CBI is significantly lower than the simulated reflectance, which may be caused by our RTM assumptions, as will be discussed later on. This discrepancy in absolute reflectance values between the modeled and the observed reflectance supports the use of the SAM as the most appropriate strategy for model inversion because SAM relies on directions of spectral vectors and not on absolute values. The higher CBI values show a closer fit between observed and simulated reflectance.

### *Performance of Simulation Models for Retrieval of CBI*

Table 6 presents the results for the estimation of CBI using the inversion of simulated values for the Landsat-TM images. All Pearson r values are highly significant and provide coherent trends. Slope is close to 1 for the post-fire scenarios (single, extended, and supervised), while it is lower for the multitemporal simulation. The multi-temporal scenario also has the lowest r value, which is mainly caused by the small sensitivity of the model to low CBI values. The slope values of less than 1 indicate that underestimations occurred frequently

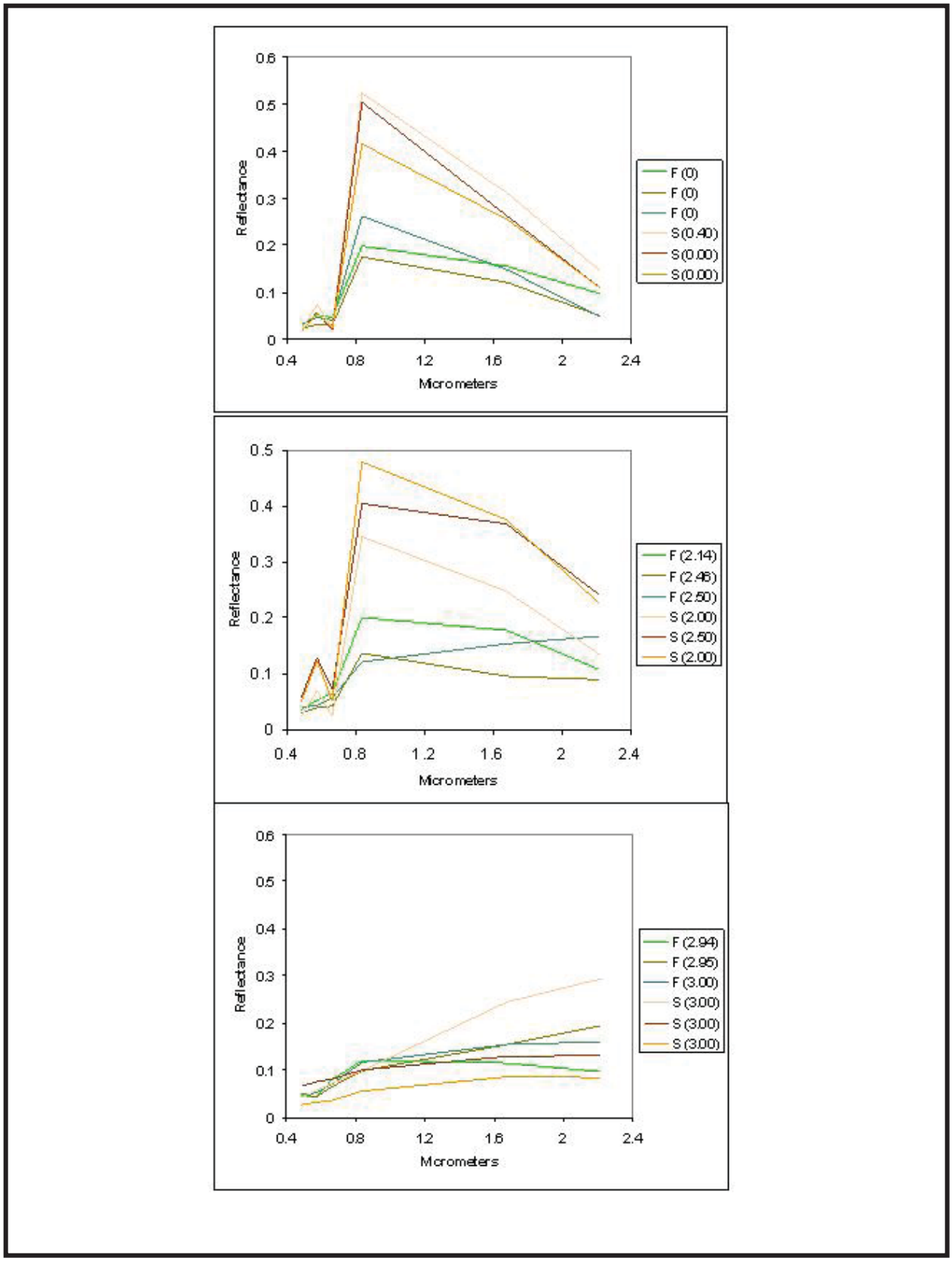


**Figure 6.** Comparison of simulated spectra and actual TM data for several ranges of CBI values.

**Table 6.** Correlation and regression values for the inversion of CBI values in the different simulation scenarios.

| Scenario | Pearson r | Intercept | Slope | Standard Error | Min Residual | Max Residual | Significance |
|---|---|---|---|---|---|---|---|
| First (single post-fire) | 0.709 | -0.004 | 0.951 | 0.550 | -1.867 | 1.189 | $p < 0.001$ |
| Second (extended post-fire) | 0.639 | 0.165 | 0.949 | 0.599 | -2.443 | 0.966 | $p < 0.001$ |
| Third (multitemporal) | 0.486 | 1.335 | 0.588 | 0.683 | -2.746 | 1.018 | $p < 0.001$ |
| Fourth (supervised) | 0.793 | 0.279 | 0.858 | 0.474 | -1.771 | 1.075 | $p < 0.001$ |

for all scenarios. The standard errors of the estimation are in the range of 0.47 to 0.68. This is about one sixth of the total CBI range, which implies that CBI values can be estimated with fairly good accuracy. The best results were obtained in the fourth (supervised) scenario, where only a selected set of substrate, PFA and PCC combinations, were extracted. This scenario is by far the simplest one because it only requires 25 reference spectra and performs better than others, especially when considering the total correlation, standard error, and average extreme residuals. Figure 7 shows a map of the study case with the spatial variation of CBI values for this fourth simulation scenario. The spatial patterns show a good agreement with field-observed severities, especially for the upper part of the CBI scale.

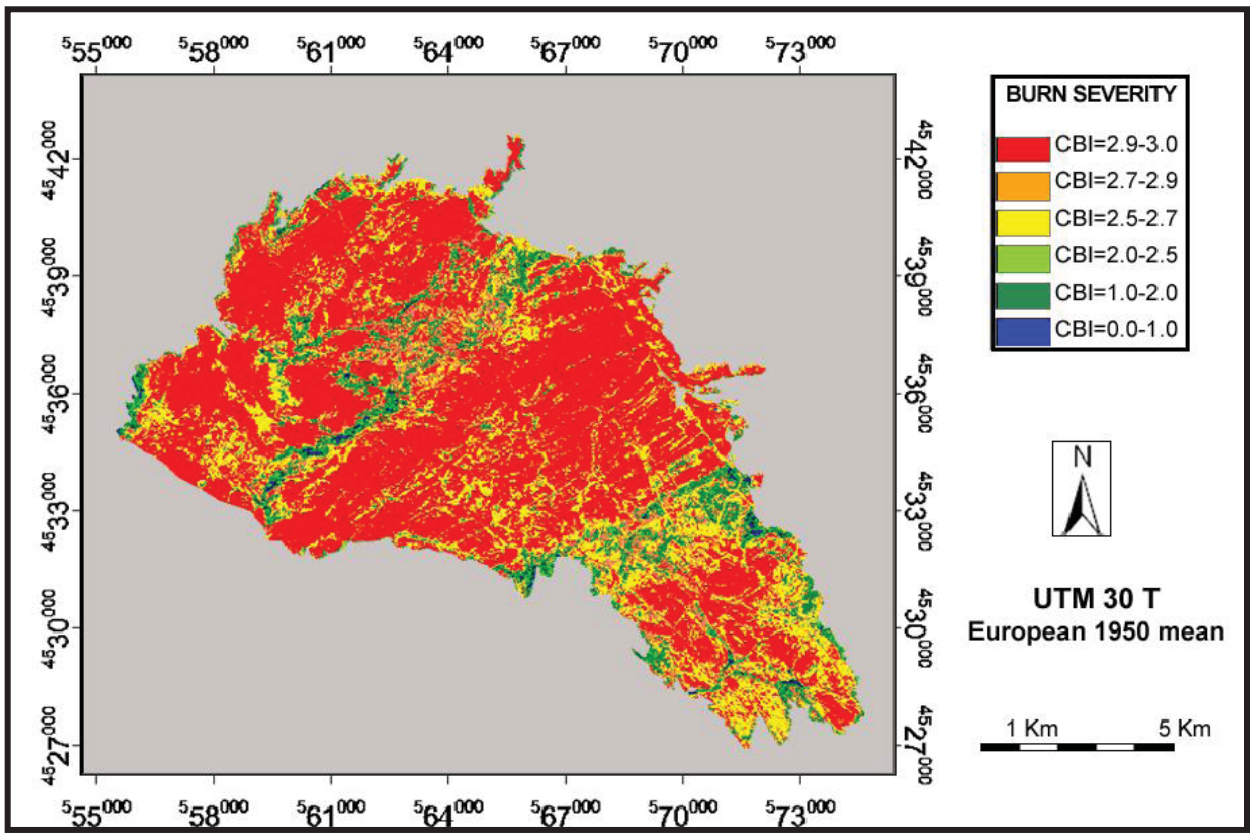


**Figure 7.** Estimation of CBI values for the study area from the inversion of the fourth simulation scenario (supervised) with Landsat-TM images.

### *Comparison of Sensors*

Using the LUT generated for the supervised simulation scenario, inversion techniques were applied to the other images of our study case. The spectral library created for the LUT was convolved to the center wavelengths of the SPOT-HRV, IRS-AWIFS, ENVISAT-MERIS and TERRA-MODIS sensors. The results are included in Figure 8, which shows the scattergraph betweeen observed and predicted CBI values for the different sensors. The higher accuracy was obtained by the Landsat-TM reflectance data, which has the best compromise between spectral and spatial resolution of all images used. The second best result was obtained from AWIFS data, instead of the SPOT-HRV, as we had hypothesized. In spite of having the same spectral resolution, the finer pixel size of SPOT-HRV apparently tends to create more spatial variability, which confounds estimation problems.

The coarser resolution data perform generally well, with $r^2$ values in the range of 0.5. MERIS offers a greater sensitivity than MODIS, which is likely caused by both greater spectral and spatial resolution. In general, all sensors analyzed tend to underestimate the CBI value, with regression intercepts between 0.7 and 2.2.

## DISCUSSION

This paper has presented several approaches to the use of RTM simulation for burn severity estimation using different satellite images. The study has shown the common advantages and disadvantages of simulation models in the interpretation of remotely sensed images.

The most important disadvantages refer to the complexity of selecting and parametrizing the RTM so it can provide a similar pattern to observed reflectance. As it was shown in Figure 6, the actual reflectance values clearly differ from modeled values in the lower part of the CBI scale, which is when vegetation is greener and more dense. This problem may be associated to the Kuusk model assumptions. Kuusk's is a canopy model, and therefore, when simulated and pixel reflectances are compared, it is assumed that each pixel is fully covered by a canopy. In the case of forested areas, this assumption implies that shade and soil are only affecting the canopy but not the areas outside the canopy. Typically, a Landsat-TM pixel would be a combination of vegetation canopies (one or several, depending on vertical structure, but this is taken into account in the Kuusk model), soil background, and shadows. When the canopy cover is close to 100%, this assumption may be valid. However, in other cases where the canopy is sparse such as in our area, the assumption is not as valid. Consequently, the use of landscape scale or geometric models (such as Geosail, GORT, DART) that account for discontinuous canopies would be more desirable. However, these models do not provide simulation for vertical stratification, which is very important in burn severity determination, and was one of the reasons for our selection of the Kuusk model.

In any case, regardless of the canopy versus landscape approach, our simulations perform well in modeling spectral shape across all the bands. In this respect, tendencies between simulated and observed spectral shape are more similar than absolute reflectance values, which supports the use of the Kuusk model as a first approximation to burn severity simulation.

As far as parameterization is concerned, this paper has explored the use of four simulation scenarios, testing a wide range of assumptions regarding burn conditions. It has been shown that extending the range of input conditions does not necessarily improve the results of inversion, but rather it decreases them. The ill-posed problem (Combal *et al.* 2002) of model inversion may be behind this lack of improvement because very similar reflectance patterns can be derived from different CBI values and that introduces noise into the inversion process. Therefore, additional efforts are required to obtain models

and simulation scenarios that can be more confident in providing consistent reflectance signatures for specific burn severities. As far as multitemporal change is concerned, the reduction of accuracy with respect to the supervised post-fire simulation scenario is probably caused by the multiplying effect of potential noises introduced by radiometric correction in pre-fire and post-fire images.

In spite of all these difficulties, it has been demonstrated that model inversion is a quick and universal mechanism to estimate CBI values because it is sensor and site independent. The same simulation scenario was applied with consistent results with different sensors. Only one study case has been presented here, but the physical basis of our simulation should be applicable to other fires with similar ecosystem characteristicas: ie., Mediterranean fires. In any case, it is important to emphasize that model inversion does not require any field data, assuming of course that the model is properly parameterized and validated. In other words, the relations are not dependent on the specific burn conditions, but are associated to ecophysiological changes caused by fire (changes in soil background, leaf color or leaf cover proportion).

As far as accuracy concerns, the supervised scenario provided similar results to other study cases based on empirical equations with an $r^2$ close to 0.65. For instance, Cocke *et al.* (2005) obtained 73% to 75% agreement to estimates CBI from Landsat multitemporal images using an empirical model with the Normalized Burn Ratio (NBR) in Arizona. Similarly, Epting *et al.* (2005) found $r^2$ correlations between 0.63 and 0.9 again using the CBI and the NBR in Alaska boreal forest, while van Wagtendonk *et al.* (2004) found $r^2$ values of 0.83 in the Yosemite National Park, although they used a polynomial model to relate CBI and changes in NBR. In this context, the simulation scenarios provide a good alternative to derive CBI estimations from empirical models as the field measurements can be focused on validating the results.

Future improvements of this simulation approach should include new models that take into better account the shade and soil variation to be expected in forested areas within a pixel. Geometrical and hybrid models should be tested in this regard. Additional effort is also needed to parameterize the input variables to reduce factors of noise that have been observed in our full range simulations.

In summary, this paper has shown that simulation models have a great potential in burn severity estimation. First, because they provide a physical explanation for relations observed empirically, they make it possible to generalize local findings. Secondly, they reduce the amount of field work required to extract severity information from remote sensing images because the interpretation is not based on statistical fitting. Finally, they provide a much wider range of conditions than those that are commonly observed in a single fire, regardless of fire behavior patterns, since the output conditions can be simulated for a wide range of scenarios. The main drawbacks of simulation models are the complexity of their formulation and calibration.

## ACKNOWLEDGEMENTS

This paper was originally presented at the 2006 Fire Ecology and Management Congress, San Diego. The main author received financial support from the organization, as well as from the sabbatical program of the University of Alcalá. This research is also part of our work in the Preview European Project (www.preview-risk.com).

## LITERATURE CITED

Brewer, C.K., J.C. Winne, R.L. Redmond, D.W. Opitz, and M.V. Mangrich. 2005. Classifying and mapping wildfire severity: a comparison of methods. Photogrammetric Engineering and Remote Sensing 71: 1311-1320.

Chavez, P.S. 1996. Image-based atmospheric corrections: revisited and improved. Photogrammetric Engineering and Remote Sensing 62: 1025-1036.

Chuvieco, E., D. Cocero, I. Aguado, A. Palacios-Orueta, and E. Prado. 2004. Improving burning efficiency estimates through satellite assessment of fuel moisture content. Journal of Geophysical Research - Atmospheres 109: 1-8.

Chuvieco, E., D. Riaño, F.M. Danson, and M.P. Martín. 2006. Use of a radiative transfer model to simulate the post-fire spectral response to burn severity. Journal of Geophysical Research - Biosciences 111: 1-15.

Cocke, A.E., P.Z. Fule, and J.E. Crouse. 2005. Comparison of burn severity assessments using Differenced Normalized Burn Ratio and ground data. International Journal of Wildland Fire 14: 189-198.

Combal, B., F. Baret, M. Weiss, A. Trubuil, D. Mace, A. Pragne`re, R. Myneni, Y. Knyazikhin, and L. Wang. 2002. Retrieval of canopy biophysical variables from bidirectional reflectance using prior information to solve the ill-posed inverse problem. Remote Sensing of Environment 84: 1-15.

Danson, F.M., and P. Bowyer. 2004. Estimating live fuel moisture content from remotely sensed reflectance. Remote Sensing of Environment 92: 309-321.

De Santis, A., and E. Chuvieco. 2006. Burn severity estimation from remotely sensed data: performance of simulation versus empirical models. Remote Sensing of Environment 108: 422-435.

Díaz-Delgado, R., F. Lloret, and X. Pons. 2003. Influence of fire severity on plant regeneration by means of remote sensing imagery. International Journal of Remote Sensing 24: 1751-1763.

Díaz-Delgado, R., X. Pons, and F. Lloret. 2001. Fire severity effects on vegetation recovery after fire. The Bigues i Riells wildfire case study. Pages 152-155 in: E. Chuvieco and M.P. Martín, editors. 3rd International Workshop on Remote sensing and GIS applications to Forest Fire Management. New methods and sensors. EARSeL, Paris, France.

Epting, J., D.L. Verbyla, and B. Sorbel. 2005. Evalation of remotely sensed indices for assessing burn severity in interior Alaska using Landsat TM and ETM+. Remote Sensing of Environment 96: 328-339.

Gastellu-Etchegorry, J.P., V. Demarez, V. Pinel, and F. Zagolski. 1996. Modeling radiative transfer in heterogeneous 3-D vegetation canopies. Remote Sensing of Environment 58: 131-156.

Gastellu-Etchegorry, J.P., E. Martin, and F. Gascon. 2004. DART: a 3D model for simulating satellite images and studying surface radiation budget. Remote Sensing of Environment 25: 73-96.

Hosgood, B., S. Jacquemoud, G. Andreoli, J. Verdebout, G. Pedrini, and G. Schmuck. 1994. Leaf Optical Properties EXperiment 93 (LOPEX93). Page 21 in: European Commission, Joint Research Centre, Institute for Remote Sensing Applications.

Jacquemoud, S. 1990. PROSPECT: a model to leaf optical properties spectra. Remote Sensing of Environment 34: 74-91.

Jain, T.B., and R.T. Graham. 2004. Is forest structure related to fire severity? Yes, no, and maybe: methods and insights in quantifying the answer. Pages 217-234 in: USDA Forest Service Proceedings RMRS-P 34.

Kachmar, M., and G.A. Sanchez-Azofeifa. 2006. Detection of post-fire residuals using high- and medium-resolution satellite imagery. Forestry Chronicle 82: 177-186.

Key, C. 2005. Remote Sensing sensitivity fo fire severity and fire recovery. Pages 29-39 in: J. Riva, F. Pérez-Cabello and E. Chuvieco, editors. Proceedings of the 5th International Workshop on Remote Sensing and GIS applications to Forest Fire Management: Fire Effects Assessment. Universidad de Zaragoza, Spain, and GOFC-GOLD, EARSeL, Paris, France.

Key, C.H., and N. Benson. 2005. Landscape Assessment: Ground measure of severity, the Composite Burn Index; and remote sensing of severity, the Normalized Burn Ratio. Pages CD: LA1-LA51 in D.C. Lutes, R.E. Keane, J.F. Caratti, C.H. Key, N.C. Benson and L.J. Gangi, editors. FIREMON: Fire Effects Monitoring and Inventory System. USDA Forest Service, General Technical Report RMRS-GTR-164.

Kruse, F.A., A.B. Lefkoff, J.B. Boardman, K.B. Heidebrecht, A.T. Shapiro, P.J. Barloon, and A.F.H. Goetz. 1993. The spectral image processing (SIPS) - interactive visualization and analysis of imaging specrometer data. Remote Sensing of Environment 44: 145-163.

Kuusk, A. 2001. A two-layer canopy reflectance model. Journal of Quantitative Spectroscopy and Radiative Transfer 71: 1-9.

Lachowski, H.M., P. Hardwick, R. Griffith, A. Parsons, and R. Warbington. 1997. Faster, better data for burned watersheds needing emergency rehab. Journal of Forestry 95: 4-8.

Lentile, L.B., Z.A. Holden, A.M.S. Smith, M.J. Falkowski, A.T. Hudak, P. Morgan, S.A. Lewis, P.E. Gessler, and N.C. Benson. 2006. Remote sensing techniques to assess active fire characteristics and post-fire effects. International Journal of Wildland Fire 15: 319-345.

Li, X., A.H. Strahler, and C.E. Woodcock. 1995. A hybrid geometric optical-radiative transfer approach for modeling albedo and directional reflectance of discontinuous canopies. IEEE Transactions on Geoscience and Remote Sensing 33: 466-480.

Liang, S. 2004. Quantitative remote sensing for land surface characterization. Wiley and Sons, Hoboken, New Jersey, USA.

Michalek, J.L., N.H.F. French, E.S. Kasischke, R.D. Johnson, and J.E. Colwell. 2000. Using Landsat TM data to estimate carbon release from burned biomass in an Alaskan spruce forest complex. International Journal of Remote Sensing 21: 323-338.

Miller, J.D., and S.R. Yool. 2002. Mapping forest post-fire canopy consumption in several overstory types using multi-temporal Landsat TM and ETM data. Remote Sensing of Environment 82: 481–496.

Moreno, J.M., and W.C. Oechel. 1989. A simple method for estimating fire intensity after a burn in California chaparral. Oecologia Plantarum 10: 57-68.

Ni, W.G., X.W. Li, C.E. Woodcock, M.R. Caetano, and A.H. Strahler. 1999. An analytical hybrid GORT model for bidirectional reflectance over discontinuous plant canopies. Ieee Transactions On Geoscience And Remote Sensing. IEEE Transactions on Geoscience and Remote Sensing 37: 987-999.

North, P.R.J. 1996. Three-dimensional forest light interaction model using a MonteCarlo method. IEEE Transactions on Geoscience and Remote Sensing 34: 946-956.

Parra, A., and E. Chuvieco. 2005. Assessing burn severity using Hyperion data. Pages 239-244 in: J. Riva, F. Pérez-Cabello and E. Chuvieco, editors. Proceedings of the 5th International Workshop on Remote Sensing and GIS applications to Forest Fire Management: Fire Effects Assessment. Universidad de Zaragoza, Spain and GOFC-GOLD, EARSeL, Paris, France.

Pereira, J.M.C., B. Mota, J.L. Privette, K.K. Caylor, J.M.N. Silva, A.C.L. Sa, and W. Ni-Meister. 2004. A simulation analysis of the detectability of understory burns in miombo woodlands. Remote Sensing of Environment 93: 296-310.

Pereira, J.M.C., A.C.L. Sa, A.M.O. Sousa, J.M.N. Silva, T.N. Santos, and J.M.B. Carreiras. 1999. Spectral characterisation and discrimination of burnt areas. Pages 123-138 in E. Chuvieco editor. Remote Sensing of Large Wildfires in the European Mediterranean Basin. Springer-Verlag, Berlin, Germany.

Pérez, B., and J. Moreno. 1998. Methods for quantifying fire severity in shrubland-fires. Plant Ecology 139: 91-101.

Pinty, B., J.L. Widlowski, M. Taberner, N. Gobron, M.M. Verstraete, M. Disney, F. Gascon, J.P. Gastellu, L. Jiang, and A. Kuusk. 2004. Radiation Transfer Model Intercomparison (RAMI) exercise: results from the second phase, 109, D06210, doi:06210.01029/02003JD004252.

Riaño, D., E. Chuvieco, F.J. Salas, and I. Aguado. 2003. Assessment of Different Topographic Corrections in Landsat-TM Data for Mapping Vegetation Types. IEEE Transactions on Geoscience and Remote Sensing 41: 1056-1061.

Riaño, D., P. Vaughan, E. Chuvieco, P. Zarco-Tejada, and S.L. Ustin. 2005. Estimation of fuel moisture content by inversion of radiative transfer models to simulate equivalent water thickness and dry matter content: analysis at leaf and canopy level. IEEE Transactions on Geoscience and Remote Sensing 43: 819-826.

Rogan, J., and J. Franklin. 2001. Mapping wildfire burn severity in Southern California forests and shrublands using enhanced Thematic Mapper imagery. Geocarto International 16: 89-99.

Rogan, J., and S.R. Yool. 2001. Mapping fire-induced vegetation depletion in the Peloncillo Mountains, Arizona and New Mexico. International Journal of Remote Sensing 22: 3101-3121.

Roy, D., Y. Jin, P. Lewis, and C. Justice. 2005. Prototyping a global algorithm for systematic fire-affected area mapping using MODIS time series data. Remote Sensing of Environment 97: 137-162.

Roy, D., and T. Landmann. 2005. Characterizing the surface heterogeneity of fire effects using multi-temporal reflective wavelength data. International Journal of Remote Sensing 26: 4197-4218.

Roy, D., P.E. Lewis, and C.O. Justice. 2002. Burned area mapping using multi-temporal moderate spatial resolution data—a bi-directional reflectance model-based expectation approach. Remote Sensing of Environment 83: 263-286.

Roy, D.P., L. Boschetti, and S.N. Trigg. 2006. Remote sensing of fire severity: assessing the performance of the Normalized Burn Ratio. IEEE Geoscience and Remote Sensing Letters 3: 112-116.

Ruiz-Gallardo, J.R., S. Castaño, and A. Calera. 2004. Application of remote sensing and GIS to locate priority intervention areas after wildland fires in Mediterranean system: a case study from south-eastern Spain. International Journal of Wildland Fire 13: 241-252.

Sa, A.C.L., J.M.C. Pereira, and J. Silva. 2005. Estimation of combustion completeness based on fire-induced spectral reflectance changes in a dambo grassland (Western Province, Zambia). International Journal of Remote Sensing 26: 4185-4195.

Scurlock, J.M.O., G.P. Asner, and S.T. Gower. 2001. Worldwide historical estimates of leaf area index, 1932–2000. Oak Ridge National Laboratory Technical Report ORNL/TM-2001/268.

Trigg, S., and S. Flasse. 2000. Characterizing the spectral-temporal response of burned savannah using in situ spectroradiometry and infrared thermometry. International Journal of Remote Sensing 21: 3161-3168.

Turner, M.G., W.W. Hargrove, R.H. Gardner, and W.H. Romme. 1994. Effects of fire on landscape heterogeneity in Yellowstone National Park, Wyoming. Journal of Vegetation Science 5: 731-742.

van Wagtendonk, J.W., R.R. Root, and C.H. Key. 2004. Comparison of AVIRIS and Landsat ETM+ detection capabilities for burn severity. Remote Sensing of Environment 92; 397-408.

White, J.D., K.C. Ryan, C.C. Key, and S.W. Running. 1996. Remote sensing of forest fire severity and vegetation recovery. International Journal of Wildland Fire 6: 125-136.

Zarco-Tejada, P.J., J.R. Miller, T.L. Noland, G.H. Mohammed, and P.H. Sampson. 2001. Scaling-up and model inversion methods with narrowband optical indices for chlorophyll content estimation in closed forest canopies with hyperspectral data. IEEE Transactions on Geoscience and Remote Sensing 39: 1491-1507.